Int. J. Heat Mass Transfer. Vol. 29, No. 10, pp. 1503–1512, 1986
Printed in Great Britain

0017-9310/86 $3.00 + 0.00
Pergamon Journals Ltd.

Simultaneous heat and mass transfer with phase change in a porous slab

SHAHRYAR MOTAKEF and MAHER A. EL-MASRI
Department of Mechanical Engineering, Massachusetts Institute of Technology, Cambridge, MA 02139, U.S.A.

(*Received* 27 *January* 1986 *and in final form* 25 *April* 1986)

Abstract—Simultaneous heat and mass transfer with phase change in a porous slab has been analytically investigated. Two spatially-steady regimes, corresponding to immobile and mobile condensate, are discovered. Closed-form analytical expressions for the temperature, vapor concentration, condensation rate and liquid-content distributions as well as the location of the condensation region for each of the two regimes is obtained.

INTRODUCTION

SIMULTANEOUS transport of heat and mass with phase change is of practical importance in applications such as the design of energy efficient buildings. With improvements in the control of air-infiltration and increasing levels of thermal insulation, the transport of vapor across the building shell and its possible condensation in the insulation increases the thermal conductivity of the building envelope and may cause structural damage.

The diverse aspects of simultaneous heat and mass transfer have been the subject of considerable analytical and experimental studies [1–4]. However, most of the analyses on condensation of vapor in open-pore insulations [5–7] neglect the coupling between heat and vapor transfer in the region where condensation occurs, as well as the effects of condensate motion. One of the more complete analyses is due to Ogniewicz and Tien [8], in which the convective contributions as well as the coupling between heat and vapor transport are taken into account. This analysis does not consider diffusion of the condensate and is, therefore, restricted to the time period over which the condensate is in a pendular state. Furthermore, as the resulting equations are solved numerically, the findings are not general.

In this paper, the phenomenon of one-dimensional simultaneous heat and mass transport with phase change in a porous slab is considered. Closed-form approximate solutions for the temperature, vapor concentration and liquid-content profiles for the cases of immobile and mobile condensate are obtained.

PROBLEM STATEMENT

We consider one-dimensional diffusion of heat, vapor and liquid in a porous slab of thickness L_T, Fig. 1. The temperature and vapor concentration boundary conditions are (T_h, C_h) and (T_c, C_c), respectively. With T_h and C_h larger than T_c and C_c, heat and vapor diffuse towards the colder boundary. For a constant pressure system, the concentration of vapor at isothermal equilibrium with liquid, C^*, is a unique function of temperature.† Therefore, the vapor saturation–concentration profile in the medium is defined by the temperature distribution. Depending on the values of the prescribed concentration conditions at the boundaries, the vapor concentration profile may touch the saturation concentration profile in the slab. The diffusing vapor would, then, undergo phase change and condense in some region of the slab. In this paper we treat the situation where the boundary conditions allow this to occur.

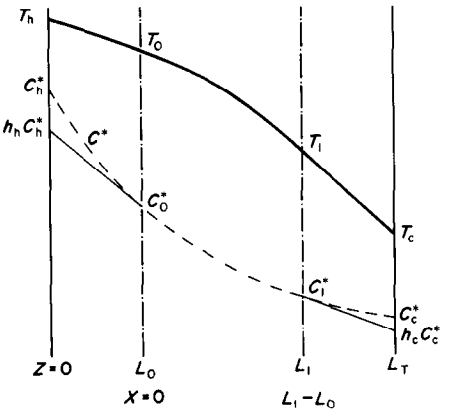

FIG. 1. Schematic of profiles of temperature and concentration in the porous slab.

At the limit where the vapor concentration at the two boundaries are at the saturation level, condensation occurs over the entire width of the slab. With the vapor concentration at the boundaries less than the saturation values, condensation occurs over some region in the slab, the wet zone, separated from the boundaries by two dry zones as illustrated in Fig. 1.

† It is assumed that the pore size is such that interfacial curvature has a negligible effect on pressure.

NOMENCLATURE

C	vapor concentration
C^*	saturation vapor concentration
c	specific heat
$D_{L,v}$	diffusivity of liquid and vapor, respectively
D_{LM}	mean liquid diffusivity
Fo_L	Fourier number based on liquid diffusivity, $D_{LM}t/L^2$
Fo_v	Fourier number based on vapor diffusivity, $D_v t/L^2$
h_{fg}	latent heat of condensation
J	liquid flux
$\bar{J}$	non-dimensional liquid flux, $Jh_{fg}/K(T_h - T_c)$
K	thermal conductivity
Le	Lewis number
L_0	location of the warm boundary of the condensation region
L_1	location of the cold boundary of the condensation region
L_T	total length of the slab
M	ratio of vapor diffusivity to liquid diffusivity
T_r	reference temperature, $(T_h + T_c)/2$
T_r'	reference temperature, $(T_0 + T_1)/2$
q	heat flux per unit area
$\bar{q}$	non-dimensional heat flux, $qL_T/k(T_h - T_c)$
V	velocity of the condensate
u	boundary condition variable, equation (30)
x	length-scale in condensation region
z	length-scale in the slab.

Greek symbols

α	thermal diffusivity
β	non-dimensional temperature drop, $(T_h - T_c)/T_r$
β'	non-dimensional temperature drop, $(T_0 - T_1)/T_r'$
γ	$h_{fg}/(RT_r)$
δ	void fraction of the porous slab
η	dimensionless temperature
θ	liquid content
θ_c	critical liquid content
κ	liquid diffusivity
λ	latent heat transport coefficient
ρ	density of air
ρ_c	density of condensate
Γ	condensation rate per unit volume
Ω'	Kossovitch number
Ω	Kossovitch number, $h_{fg}C_r^*/\rho c_p T_r$.

Subscripts

c	cold
h	hot
g	gas
l	liquid
s	steady state
t	transient
v	vapor
0	variable associated with L_0
1	variable associated with L_1.

Superscripts

¯	non-dimensionalized variable
′	parameter evaluated in reference to the condensation region.

The condensation of vapor in the wet zone can be considered to be simultaneously a vapor sink, liquid source and heat source. Hence, the three processes of vapor diffusion, condensate motion and heat transfer are coupled through the condensation rate. The location of the condensation region as well as the vapor concentration, liquid-content and temperature profiles in the medium are obtained by the simultaneous solution of the three coupled conservation equations for vapor, liquid and heat. The solution to this set of equations with the prescribed slab boundary conditions is obtained by partitioning the medium into three regions of dry–wet–dry. The conservation equations are solved in each region. By applying continuity of temperature and vapor concentration together with energy and mass conservation at the wet–dry boundaries, the temperature and concentration profiles in the three regions are matched.

Transport equations

In this study one-dimensional diffusive transfer of heat, vapor and liquid is considered. According to Fourier and Fick's laws, heat and vapor fluxes are given as:

$$q = -K\,\mathrm{d}T/\mathrm{d}z \tag{1}$$

$$j_v = -D_v\,\mathrm{d}C/\mathrm{d}z. \tag{2}$$

Presently, attention is focused on porous media with large pores, and thus K and D_v are taken to be spatially uniform and equal to the properties of the gas occupying the pores.

In unsaturated porous media where surface tension forces dominate gravitational effects, liquid flux, neglecting the temperature dependence of surface tension of the liquid, is [9]:

$$j_L = \rho_c \delta D_L(\theta)\,\mathrm{d}\theta/\mathrm{d}z \tag{3}$$

where θ denotes liquid content and is defined as the fraction of the pore space occupied by liquid. $D_L(\theta)$ is a phenomenologically defined liquid diffusivity whose dependence on liquid content is a complicated function of the internal geometry and structure of the

medium. In general, liquid diffusion may be modelled to consist of two regimes. At liquid contents less than the critical liquid content (CLC), liquid is in a pendular state and does not exhibit any tendency to diffuse. Beyond the CLC, as the pendular drops coalesce and the capillary pores are wetted, liquid is propelled by surface tension forces from regions of higher liquid content to the drier regions. Although liquid diffusivity in the second regime is a function of θ, for mathematical simplicity a mean value of liquid diffusivity, D_{LM}, is used in the problem formulation. Thus, liquid diffusivity is modelled separately for each of the two regimes as:

(1) Immobile condensate

$$\theta < \theta_c \quad D_L(\theta) = 0.\dagger$$

(2) Mobile condensate

$$\theta > \theta_c \quad D_L(\theta) = D_{LM}.$$

Conservation equations and model

In the absence of any convective contributions [9], the conservation equations for heat, vapor and liquid may be written as:

$$K\frac{d^2T}{dz^2} + \Gamma h_{fg} = \rho_c \frac{\partial T}{\partial t} \tag{4}$$

$$D_v \frac{\partial^2 C}{\partial z^2} - \Gamma = \frac{\partial C}{\partial t} \tag{5}$$

$$\rho_c \delta \frac{\partial}{\partial z}\left[D_L(\theta)\frac{\partial \theta}{\partial z}\right] + \Gamma = \rho_c \delta \frac{\partial \theta}{\partial t} \tag{6}$$

subject to the boundary conditions:

$$\text{at} \quad z = 0 \quad T = T_h, \quad C = C_h$$

$$\text{at} \quad z = L_T \quad T = T_c, \quad C = C_c.$$

In the wet zone the conservation equations are coupled through the condensation rate term, Γ, whereas in the dry zone $\Gamma = 0$ and $\theta = 0$. Beyond the initial transient ($\alpha t/L_T^2 \gg 1$, $D_v t/L_T^2 \gg 1$), the temperature and vapor concentration profiles remain invariant with time, vapor condenses continuously in the medium, the condensate accumulates with time, and for liquid contents less that CLC remains immobile. (In this work any condensation that occurs during the initial transient is neglected.) Therefore, equation (6) simplifies to

$$\frac{\partial \theta}{\partial t} = \frac{\Gamma(z)}{\rho_c \delta} \qquad \theta < \theta_c \tag{7}$$

and we define the solution which satisfies the above conditions as the first spatially-steady regime. During this regime the temperature and concentration profiles are at steady state, there is no condensate motion, the liquid content in the wet zone increases linearly with time, and the location of the condensation region is spatially fixed and determined by the continuity of heat and vapor fluxes at the wet–dry boundaries. After a time scale of order $(\theta_c \rho_c \delta/\Gamma)$ the local values of θ reach CLC, and liquid diffusion leads to the migration of the condensate into the dry regions and the subsequent expansion of the condensation region. Eventually, after a time period of order $[(L_T^2/D_{LM}) + (\theta_c \rho_c \delta/\Gamma)]$ a new steady state is established, allowing equation (6) to be simplified to

$$\frac{d^2\theta}{dz^2} = -\frac{\Gamma(z)}{\rho_c \delta D_{LM}} \qquad \theta > \theta_c. \tag{8}$$

This regime is defined as the second spatially-steady regime. Now, the vapor that condenses in the wet zone diffuses towards the wet zone's boundaries as liquid and re-evaporates at these boundaries leaving the liquid-content profile invariant with time. The heat and vapor flux conservation conditions at the wet zone's boundaries, that determine the location and boundary temperature of the condensation region, account for the discontinuities of heat and vapor flux associated with phase change at those boundaries.

In light of the non-uniform liquid content distribution in the first regime [see equation (22)], the analysis of the unsteady regime that separates the two steady regimes can be only achieved numerically, and is not undertaken in this study.

SOLUTIONS

As the effects of condensate motion on the temperature distribution in the slab can be neglected [9], the second spatially-steady regime lends itself to similar analytical treatment as the first. Equations (4) and (5) govern both spatially-steady regimes with the right-hand terms set to zero. The differences between the first and second regimes is in the simplification of equation (6) to either (7) or (8) as well as in the matching conditions at the wet–dry interfaces. We begin, therefore, by obtaining a general solution for the wet zone profiles.

Condensation region profiles

Referring to Fig. 1, we consider a wet zone of some thickness $L_1 - L_0$, boundary temperatures T_0 and T_1, and corresponding boundary concentrations $C_0^*(T_0)$ and $C_1^*(T_1)$. The vapor and energy continuity equations are coupled through the condensation rate term. By eliminating this term equations (4) and (5) are reduced, for steady state, to

$$\frac{d^2T}{dx^2} + \frac{h_{fg} D_v}{k}\frac{d^2C^*}{dx^2} = 0. \tag{9}$$

Condensation occurs throughout the width of the region and, hence, the vapor concentration is a unique function of the temperature distribution. Therefore, equation (9) is a differential equation in terms of

† This condition is more restrictive than is required. A less conservative condition on liquid diffusivity necessary for neglecting condensate diffusion is obtained in ref. [9].

temperature only. The functional dependence of saturation concentration on temperature is obtained by invoking the Clausius–Clapeyron relationship. By approximating the vapor as a perfect gas and recognizing that $v_g \gg v_f$, the Clausius–Clapeyron equation may be well approximated by

$$\frac{dC^*}{dT} \cong \frac{h_{fg} C^*}{RT^2}. \tag{10}$$

Equation (10) is integrated from $C_r^{*\prime}$ corresponding to the vapor concentration at the mean temperature of the wet zone, $T_r' = (T_0 + T_1)/2$, to C^* at T:

$$\frac{C^*}{C_r^{*\prime}} = \exp\left[\frac{h_{fg}}{RT_r'}\left(1 - \frac{T_r'}{T}\right)\right]. \tag{11}$$

By non-dimensionalizing temperature in the condensation region as:

$$\eta' = (T - T_r')/(T_0 - T_1) \tag{12}$$

equation (11) is succinctly written as:

$$C^*/C_r^{*\prime} = \exp(\Phi) \tag{13}$$

where

$$\Phi = \frac{v'\beta'\eta'}{1 + \beta'\eta'}$$
$$v' = h_{fg}/(RT_r') \quad \text{and} \quad \beta' = \Delta T'/T_r'. \tag{14}$$

Introducing equations (11) and (13) into the energy equation, (9), and non-dimensionalizing the length scale in the condensation region as $\bar{x} = x/(L_1 - L_0)$, the following second-order non-linear differential equation for reduced temperature is obtained:

$$\left\{1 + \frac{\Omega' v'}{Le}(1 + \beta'\eta')^{-2}\exp[\Phi]\right\}\frac{d^2\eta'}{d\bar{x}^2} + \left\{\frac{v'\beta'\Omega'}{Le}(1 + \beta'\eta')^{-2}\exp[\Phi]\right\}\left(\frac{d\eta'}{d\bar{x}}\right)^2 = 0$$

where

$$Le \text{ (Lewis number)} = \alpha/D_v$$
$$\Omega' \text{ (Kossovitch number)} = (h_{fg} C_r^{*\prime}/\rho c_p T_r'). \tag{15}$$

Equation (15) is subject to the following boundary conditions:

$$\eta' = 1/2 \quad \text{at } \bar{x} = 0$$
$$\eta' = -1/2 \quad \text{at } \bar{x} = 1 \tag{16}$$

and may be solved numerically. However, an approximate analytical solution is obtained by linearizing it around a zeroth-order linear temperature profile

$$\eta' = 0.5 - \bar{x} + \varepsilon(\bar{x}) \tag{17}$$

where $\varepsilon(x)$ is a temperature perturbation satisfying

$$\varepsilon^2 \ll 1, \quad \varepsilon(\bar{x} = 0) = \varepsilon(\bar{x} = 1) = 0. \tag{18}$$

Introducing equation (17) into (15) and neglecting terms of order ε^2, the following second-order linear differential equation in ε is obtained:

$$\frac{d^2\varepsilon}{d\bar{x}^2}\left(1 + \frac{\Omega' v'}{Le}\right) + \frac{d\varepsilon}{d\bar{x}}\left(\frac{-2v'^2\beta'\Omega'}{Le}\right) + \frac{v'^2\beta'\Omega'}{Le} = 0. \tag{19}$$

Solving the above in conjunction with boundary conditions (18) and introducing the result into equation (17) yields:

$$\eta' = 0.5\left[1 - \bar{x} - \frac{\exp(\lambda'\bar{x}) - 1}{\exp(\lambda') - 1}\right] \tag{20}$$

where

$$\lambda' = \frac{2v'^2\beta'\Omega'}{Le + v'\Omega'}.$$

The above is an approximate but general solution for $\eta'(x)$. It indicates that the temperature profile in the wet zone is a function of one parameter only, λ', which is the ratio of heat released by condensation to heat conducted across the wet zone in absence of condensation and is, therefore, called the latent heat transport coefficient [9]. The reduced temperature $\eta'(x)$ is plotted for various values of λ' in Fig. 2. The accuracy of the perturbation solution is established by comparing it with the numerical solution of equation (15) for two λ' values of 2.04 and 4.12 (corresponding to temperature drops of 20°C and 40°C, respectively; see Figs. 3 and 4). The results indicate that as the value of λ' is increased the analytical solution diverges from the numerical result due to the increased effect of terms of order ε^2 and higher powers. As the range of values for λ' corresponding to condensation of vapor in insulated structures does not exceed 6, equation (20) is a good analytical approximation to the temperature profile in the condensation region.

The condensation rate per unit volume in non-dimensional form can be obtained from equations (4)

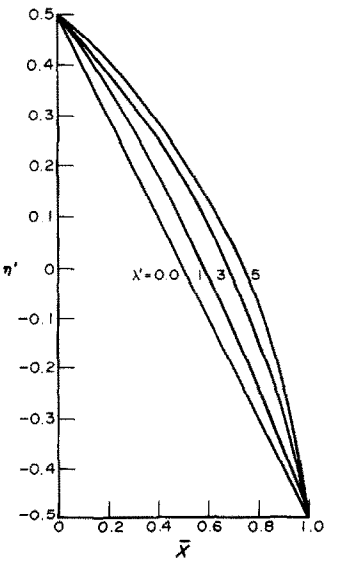

FIG. 2. Reduced temperature profile for different values of λ'. The case of no condensation is characterized by $\lambda' = 0$.

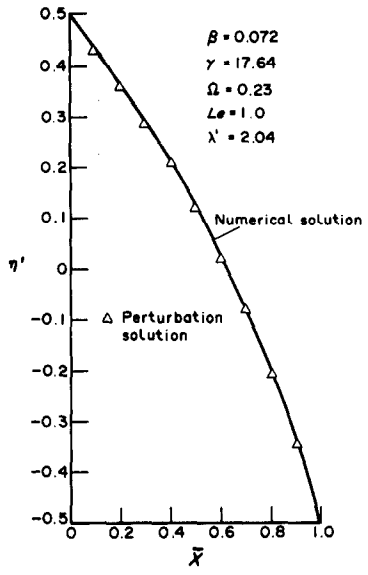

FIG. 3. Comparison of the analytical solution with the numerical results of the reduced temperature profile, $\lambda' = 2.04$.

and (20):

$$\bar{\Gamma} = \frac{Le\beta'}{\Omega'} \frac{\lambda'^2}{2} \frac{\exp(\lambda' x)}{\exp(\lambda') - 1} \tag{21}$$

indicating an exponential dependence of $\bar{\Gamma}$ on $\bar{x}$, Fig. 5. Furthermore, the condensation rate exhibits a strong dependence on the temperature drop across the zone: $\bar{\Gamma} \sim \lambda'\beta'^2 \sim \beta'^3$. Thus, a doubling of temperature drop results in an eight fold increase in the volumetric condensation rate.

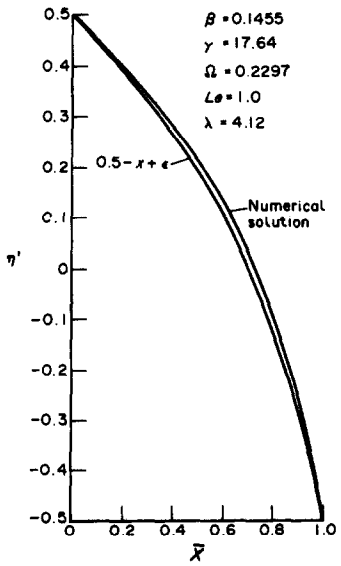

FIG. 4. Comparison of the analytical solution with the numerical results of the reduced temperature profile, $\lambda' = 4.12$.

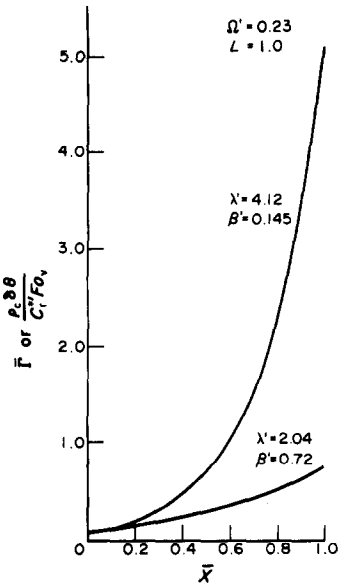

FIG. 5. Non-dimensional condensation rate and liquid-content profile for two different boundary conditions.

FIRST SPATIALLY-STEADY SOLUTION

During the first spatially-steady regime the liquid-content distribution in the wet zone is obtained by integration of equation (6):

$$\theta(\bar{x}, Fo_v) = \left[\frac{C^{*\prime}r}{\rho_c\delta} \frac{Le\beta'}{\Omega'} \frac{\lambda'^2}{2} \frac{\exp(\lambda' x)}{\exp(\lambda') - 1}\right] Fo_v \tag{22}$$

where Fo_v is the Fourier number based on vapor diffusivity, $D_v t/(L_1 - L_0)^2$. The liquid-content distribution increases linearly with time and follows the same profile as condensation rate. An example is shown in Fig. 5, except for a change of the label on the vertical axis $\bar{\Gamma}$ to $\rho_c\delta\theta/C_r^{*\prime}Fo_v$.

Matching of zones

The analytical expressions for the temperature and liquid-content profiles in the condensation region depend on the width and temperature boundary conditions of the wet zone. These parameters are not known *a priori* and are obtained by matching the temperature and vapor concentration profiles in the condensation region with those of the adjacent dry regions. Once these parameters are identified the analytical results of the previous section may be rescaled to reflect their parametric dependence on the slab's boundary conditions and width.

In the dry regions, the vapor concentration and temperature profiles vary linearly with position. Assuming uniform thermal conductivity and vapor diffusivity throughout the slab, continuity of heat and vapor flux across the boundaries of the condensation region is equivalent to equality of concentration and temperature gradients at the boundaries:

$$\frac{T_h - T_0}{L_0} = -\frac{dT'}{dz}, \quad z = L_0 \tag{23}$$

$$\frac{C_h - C_0^*}{L_0} = -\frac{dC^*}{dz}, \quad z = L_0 \tag{24}$$

$$\frac{T_1 - T_c}{L_T - L_1} = -\frac{dT'}{dz}, \quad z = L_1 \tag{25}$$

$$\frac{C_1^* - C_c}{L_T - L_1} = -\frac{dC^*}{dz}, \quad z = L_1. \tag{26}$$

Four unknowns are associated with the four equations (23)–(26). These are: T_0, T_1, L_0 and L_1.

Before proceeding with the solution of the four equations let a new set of non-dimensional variables and parameters be defined. These are conjugate to the previously defined variables and are referred to the slab boundary conditions and width:

$$\eta = \frac{T - [(T_h + T_c)/2]}{T_h - T_c} \tag{27}$$

$$\bar{z} = z/L_T. \tag{28}$$

The new non-dimensional temperature satisfies the boundary conditions:

$$\begin{aligned} \eta &= 0.5 \quad \text{at } \bar{z} = 0 \\ \eta &= -0.5 \quad \text{at } \bar{z} = 1. \end{aligned} \tag{29}$$

The unprimed conjugates of β' and Ω' are defined in the Nomenclature.

The values of temperature at the boundaries of the wet zone η_0 and η_1 are obtained by eliminating the length scales between the heat and vapor continuity equations (23)–(26). By invoking the Clausius–Clapeyron relation and making the simplifying approximation of $(1+\eta\beta) \sim 1$, one equation in the form of

$$1 - h_{h,c} \exp(u_{h,c}) + u_{h,c} = 0 \tag{30}$$

is obtained where

$$\begin{aligned} u_c &= \gamma\beta(\eta_c - \eta_1) < 0 \\ u_h &= \gamma\beta(\eta_h - \eta_0) > 0. \end{aligned} \tag{31}$$

A plot of equation (30) is given in Fig. 6. For a given value of humidity, h, equation (30) has two u roots: one positive and one negative. The positive root, u_h, corresponds to boundary conditions on the hot side of the slab and is associated with h_h and η_0. The negative root, u_c, corresponds to the cold-side boundary conditions and is associated with h_c and η_1. When the cold-side humidity, h_c, is put into equation (30), the negative root and when h_h is used the positive root must be used. Therefore, η_0 and η_1 are now defined, through equation (30), as a function of the slab boundary conditions, and the primed parameters which define the analytical solutions of the wet zone can be readily calculated.

The two length scales L_0 and L_1 are obtained by the simultaneous solution of any two of the four boundary

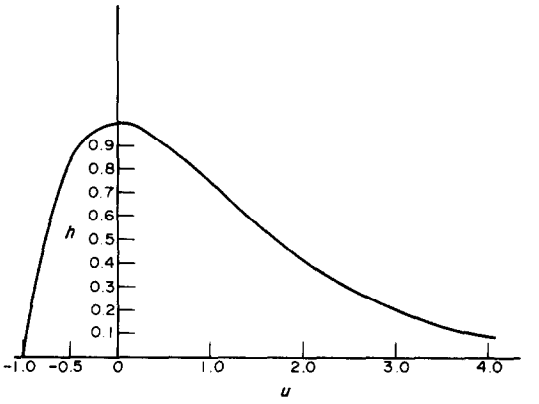

FIG. 6. Plot of boundary condition parameter vs humidity.

equations (23)–(26):

$$\bar{L}_0 = \Pi_2 \Big/ \left[\Pi_2 + \left(\frac{0.5+\eta_1}{0.5-\eta_0}\right)\Pi_1 - \left(\frac{\eta_0-\eta_1}{0.5-\eta_0}\right)\Pi_1\Pi_2 \right] \tag{32}$$

$$\bar{L}_1 = \Pi_2 \left(1 - \frac{\eta_0-\eta_1}{0.5-\eta_0}\Pi_1\right) \Big/ \left[\Pi_2 + \left(\frac{0.5+\eta_1}{0.5-\eta_0}\right)\Pi_1 - \left(\frac{\eta_0-\eta_1}{0.5-\eta_0}\right)\Pi_1\Pi_2 \right] \tag{33}$$

where

$$\Pi_1 = -\frac{1}{2}\left(\frac{\lambda'}{\exp\lambda' - 1} + 1\right) \tag{34}$$

$$\Pi_2 = -\frac{1}{2}\left(\frac{\lambda' \exp\lambda'}{\exp\lambda' - 1} + 1\right). \tag{35}$$

With the identification of the location of the condensation region the first spatially-steady regime is completely defined. The temperature, vapor concentration, liquid content distributions, as well as the condensation rate per unit volume and the location of the condensation region are obtained in closed form.

The approximate analytical results are compared, for a representative set of boundary conditions and medium properties, with the numerical solutions in Fig. 7. The numerical solution of the energy equation, is obtained by the spatial discretization of equation (15) and successive iteration, and the location of the condensation region is obtained by numerical solution of equations (23)–(26). The agreement for both the temperature profile and the location of the condensation region is very good.

SECOND SPATIALLY-STEADY REGIME

The second spatially-steady regime is defined as the regime where the condensate is mobile and the liquid content in the condensation region has reached a steady profile. The energy equation for this regime is identical to that of the first regime, and thus the non-dimensional temperature profile in the wet zone, equation (20), and volumetric condensation rate,

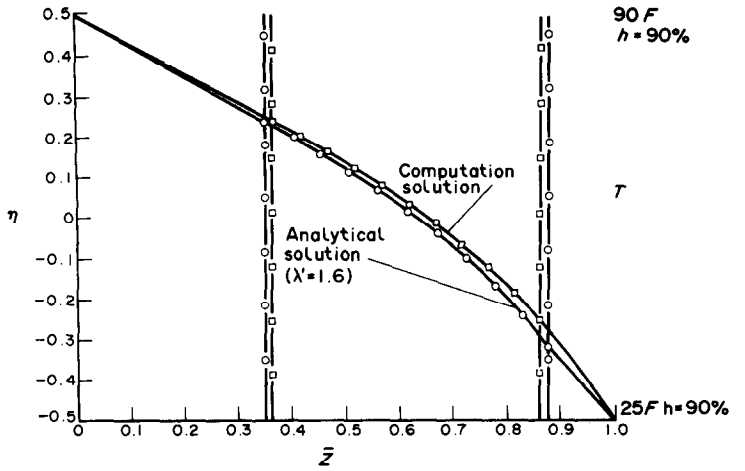

FIG. 7. Comparison of the analytical solution with the numerical results of the non-dimensional temperature profile in the slab during the first steady regime.

equation (21), of the first steady regime are equally valid in the second regime. At steady state liquid continuity for this regime is given by:

$$\frac{d^2\theta}{d\bar{x}^2} = \frac{\Gamma_{(x)}(L_0 - L_1)^2}{D_{LM}\rho_c\delta} \tag{36}$$

and as liquid diffusion is assumed to be zero for $\theta < \theta_c$, equation (36) is associated with the following boundary conditions:

$$\begin{aligned} \bar{x} = 0 \quad & \theta = \theta_c \\ \bar{x} = 1 \quad & \theta = \theta_c. \end{aligned} \tag{37}$$

Integrating equation (36) and using results of the first regime for $\bar{\Gamma}(\bar{x})$, the liquid-content distribution is obtained as:

$$\theta_s(\bar{x}) = \theta_c + M\frac{C_t'}{\rho\varepsilon}\frac{Le\beta'}{\Omega'}\left[\frac{1}{2}\left(\bar{x} - \frac{\exp\lambda'\bar{x} - 1}{\exp\lambda' - 1}\right)\right] \tag{38}$$

where M is the ratio of vapor diffusivity to liquid diffusivity. Liquid-content distribution for several values of the latent heat transport coefficient is given in Fig. 8, indicating a strong dependence on λ'. As the condensation rate, $\bar{\Gamma}$, increases with $\bar{x}$, Fig. 5, the liquid-content profiles vary steeply at the colder edge of the condensation region and therefore, the point of maximum liquid content, lies closer to the colder boundary.

During this regime the liquid efflux into the boundaries of the wet zone is equal to condensation rate per unit area of the wet zone. Liquid effluxes at $\bar{x} = 0$ and $\bar{x} = 1$, $\bar{J}_0$ and $\bar{J}_1$, respectively, are proportional to the gradient of liquid content at those locations, and are calculated to be:

$$\bar{J}_0 = \frac{Le\beta'}{\Omega'}\frac{\exp(\lambda' - 1) - \lambda'}{2(\exp\lambda' - 1)} \tag{39}$$

$$\bar{J}_1 = \frac{Le\beta'}{\Omega'}\frac{(\lambda' - 1)\exp\lambda' + 1}{2(\exp\lambda' - 1)}. \tag{40}$$

Comparison of the above two equations indicates that $\bar{J}_1$ increases much more rapidly than $\bar{J}_0$ with increasing λ'.

Matching of zones

As in the first steady regime, the vapor concentration and temperature distributions in the dry regions are linear. The continuity of heat flux and mass conservation at the two wet–dry interfaces result in four equations which are solved to generate the values of the four unknowns T_0, T_1, L_0 and L_1.

The heat supplied from the warmer side of the slab

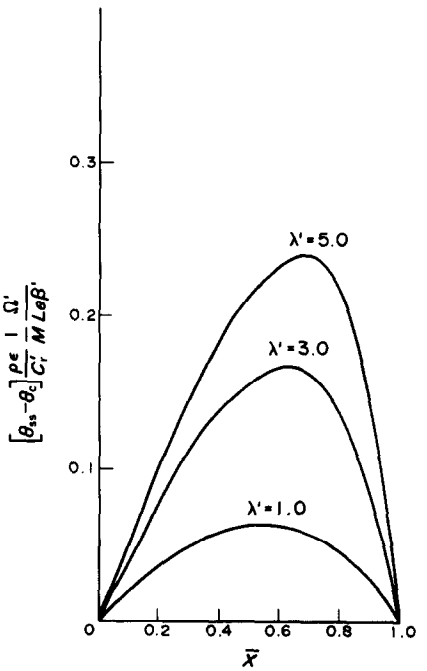

FIG. 8. Normalized steady state liquid-content profiles during the second steady regime.

to the condensation region is equal to the heat flux conducted into the wet zone plus the heat flux required to evaporate the liquid flux J_0

$$-k\frac{T_h-T_0}{L_0}=-k\frac{dT'}{dz}+J_0h_{fg},\quad z=L_0. \tag{41}$$

On the other hand, the vapor flux entering the wet zone at $z=L_0$ is equal to the sum of the vapor flux entering the slab at $z=0$ plus the vapor flux generated by the evaporation of the liquid flux J_0.

$$-D_v\frac{C_h-C_0^*}{L_0}=-\frac{dC^*}{dz}-J_0,\quad z=L_0. \tag{42}$$

By similar arguments the following heat and vapor-flux balances at the $z=L_1$ boundary of the wet zone are obtained:

$$-k\frac{T_1-T_c}{L_T-L_1}+J_1h_{fg}=-k\frac{dT'}{dz},\quad z=L_1 \tag{43}$$

and

$$D_v\frac{C_1^*-C_c}{L_T-L_1}=-D_v\frac{dC^*}{dz}+J_1,\quad z=L_1. \tag{44}$$

Under steady-state conditions, the condensed vapor migrates towards the boundaries of the condensation region and evaporates. Hence, as there is no net accumulation of condensate, the vapor flux entering the slab equals the vapor flux leaving it:

$$D_v\frac{C_1^*-C_c}{L_T-L_1}=D_v\frac{C_h-C_0^*}{L_0}. \tag{45}$$

By the same token, with no net mass change in the porous slab, there is no associated change in the internal energy of the wet zone. Therefore, the heat flux entering the slab is equal to the heat flux leaving it:

$$k\frac{T_h-T_0}{L_0}=k\frac{T_1-T_c}{L_T-L_1}. \tag{46}$$

By substituting equations (39) and (40) for liquid fluxes $\bar{J}_0$ and $\bar{J}_1$, equations (41) and (43) are reduced to:

$$\frac{\eta_h-\eta_0}{\bar{L}_0}=\frac{\eta_1-\eta_c}{1-\bar{L}_1}=1. \tag{47}$$

The above indicates that the heat flux into and out of the wet zone is equal to the heat flux through the slab with no condensation present ($\eta_h-\eta_c=1$). The invariance of heat flux across the slab to condensation of vapor is due to the evaporation of the condensate at the wet zone boundaries which counterbalances the effects of heat released by condensation in the wet zone.

Two equations relating the temperatures at the wet zone boundaries, η_0 and η_1, are obtained by eliminating the length scales between equations (41) and (42), and (43) and (44), using the Clausius–Clapeyron relation, and the wet zone temperature distribution of equation (20):

$$\frac{h_h\exp(\Phi_h)-\exp(\Phi_0)}{\eta_h-\eta_0}=0.5v\beta\left[\left(1+\frac{\lambda'}{\exp\lambda'-1}\right)(1+\eta_0\beta)^{-2}\exp(\Phi_0)-\frac{Le}{\Omega v}\left(1-\frac{\lambda'}{\exp\lambda'-1}\right)\right] \tag{48}$$

and

$$\frac{h_c\exp(\Phi_c)-\exp(\Phi_1)}{\eta_c-\eta_1}=0.5v\beta\left[\left(1+\frac{\lambda'\exp\lambda'}{\exp\lambda'-1}\right)(1+\eta_1\beta)^{-2}\exp(\Phi_1)-\frac{Le}{\Omega v}\left(1-\frac{\lambda'\exp\lambda'}{\exp\lambda'-1}\right)\right]. \tag{49}$$

In equation (48) η_1 and in equation (49) η_0 appear implicitly in λ' and their values are obtained by the simultaneous solution of the two equations by successive iteration. In Fig. 9 the dependence of η_0 and η_1 on the humidity boundary conditions at a fixed set of boundary temperatures is investigated. With the slab boundaries at 100% relative humidity, condensation occurs throughout the region and the temperature at the wet zone boundaries approach the slab boundary values ($\eta_0\to 0.5, \eta_1\to -0.5$). At lower humidity values, as the size of the wet zone gets smaller, the temperature drop across it is reduced.

The length scales of the second spatially-steady regime are obtained by the simultaneous solution of the two heat balance equations, equations (41) and (43):

$$\bar{L}_0=(\eta_h-\eta_0)\Big/\left[\frac{\Delta T'}{\Delta T}+1-(\eta_0-\eta_1)\right] \tag{50}$$

and

$$\bar{L}_1=\left[\frac{\Delta T}{\Delta T'}+(\eta_h-\eta_0)\right]\Big/\left[\frac{\Delta T'}{\Delta T}+1-(\eta_0-\eta_1)\right]. \tag{51}$$

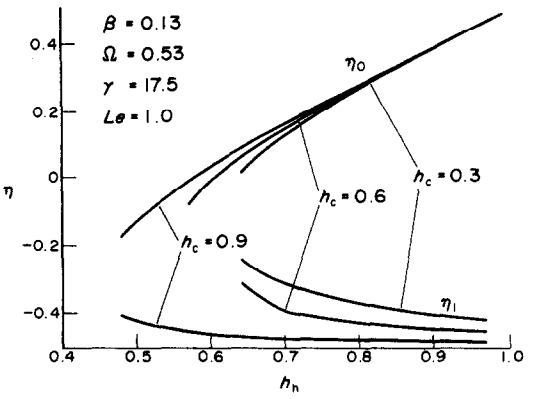

FIG. 9. Non-dimensional temperature at the boundaries of the wet zone vs the hot-side humidity.

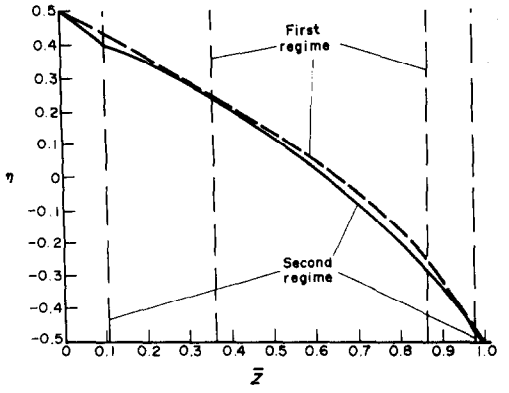

FIG. 10. Non-dimensional temperature profile in the slab during the second steady regime.

With the solution of the length scales, the second spatially-steady regime is now completely defined.

As an illustrative example the second spatially-steady regime for the parameters of Fig. 7 is investigated. The temperature profile as well as the location of the wet zone for this case is shown in Fig. 10.

SUMMARY

The temporal evolution of condensation in a porous slab consists of three regimes. During the first regime, where the condensate is immobile, the vapor concentration, temperature and location of the condensation region are spatially steady and the condensate is accumulated linearly with time. Assuming a negligible variation of thermal conductivity of the slab with increased liquid content, the energy released by the condensation of vapor reduces the magnitude of heat flux entering the slab, $\bar{q}_h$, Fig. 11. As the local values of liquid content increase above CLC and the condensate becomes mobile, the concentration and temperature profiles

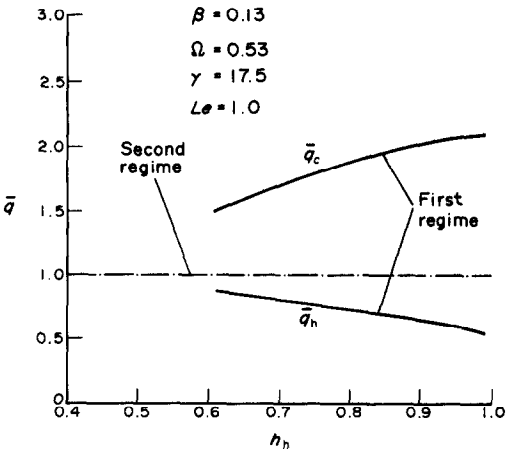

FIG. 11. Non-dimensional heat flux at the boundaries of the slab during the two regimes vs the hot-side humidity.

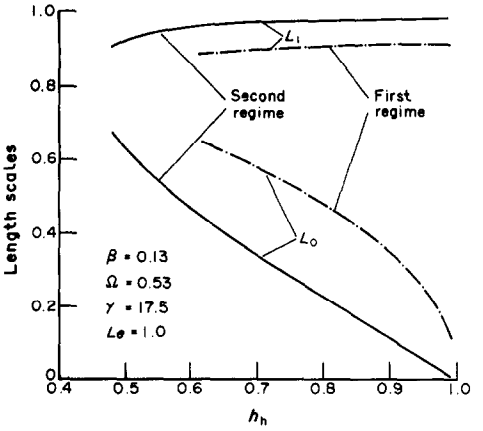

FIG. 12. Location of the condensation region during the two regimes vs the hot-side humidity.

undergo a transient change, and the condensation region expands to accommodate the motion of condensate towards its boundaries, Fig. 12. This transition period is followed by the second spatially-steady regime during which the temperature, vapor concentration and liquid-content profiles are time-invariant. During this regime the effect of heat released by condensation is negated with the absorption of energy by the evaporation of the condensate effluxes at the wet zone boundaries and therefore, the values of heat flux into and out of the slab are equal to the values for the case of no condensation, Fig. 11.

REFERENCES

1. A. V. Luikov, *Heat and Mass Transfer in Capillary Porous Bodies*. Pergamon Press, Oxford (1966).
2. J. W. Cary and S. A. Taylor, The interaction of the simultaneous diffusion of heat and water vapor, *Soil Sci. Proc.* 413–416 (1962).
3. D. A. deVries, Simultaneous transfer of heat and moisture in porous media, *Trans. Am. geophys. Un.* **39**, 909–916 (1958).
4. N. E. Edlefsen and A. B. C. Anderson, Thermodynamics of soil moisture, *Hilgardia* **15**, 31–298 (1943).
5. P. Marsh, *Thermal Insulation and Condensation*. The Construction Press, London (1979).
6. M. Bomberg, Moisture flow through porous building materials, Lund Institute of Technology, Lund, Sweden (December 1973).
7. Advisory Committee of the Building Research Advisory Board, *Cold Storage Facilities: Comprehensive Program for Research*. Division of Engineering and Industrial Research, National Academy of Science—National Research Council, Washington, DC, Publication 1099 (1963).
8. Y. Ogniewicz and C. L. Tien, Analysis of condensation in porous insulation, *Int. J. Heat Mass Transfer* **24**, 421–429 (1981).
9. S. Motakef, Simultaneous heat and mass transport with phase change in insulated structures. Ph.D. thesis, Massachusetts Institute of Technology, Cambridge, MA (1984).
10. J. R. Philip and D. A. deVries, Moisture movement in porous materials under temperature gradients, *Trans. Am. geophys. Un.* **38**, 222–232 (1957).

TRANSFERTS SIMULTANES DE CHALEUR ET DE MASSE AVEC CHANGEMENT DE PHASE DANS UNE COUCHE POREUSE

Résumé—On étudie analytiquement les transferts simultanés de chaleur et de masse avec changement de phase dans une couche poreuse. Deux régimes spatialement stables, correspondant au condensat immobile et mobile, sont découverts. On obtient des expressions analytiques pour la température, la concentration de vapeur, le flux de condensat, la distribution de teneur en humidité, aussi bien que la location de la région de condensation pour chacun des deux régimes.

GLEICHZEITIGER WÄRME- UND STOFFTRANSPORT MIT PHASEN-WECHSEL IN EINER PORÖSEN PLATTE

Zusammenfassung—Der gleichzeitige Wärme- und Stofftransport mit Phasenänderung in einer porösen Platte wurde analytisch untersucht. Es wurden zwei räumlich unveränderliche Bereiche, die unbeweglichem und beweglichem Kondensat entsprechen, entdeckt. Analytische Ausdrücke geschlossener Form wurden für die Verteilung von Temperatur, Dampfkonzentration, Kondensationsrate und Flüssigkeitsanteil und die Lage des Kondensationsgebiets in den beiden Bereichen ermittelt.

ВЗАИМОСВЯЗАННЫЙ ТЕПЛО-И МАССОПЕРЕНОС ПРИ ФАЗОВОМ ПЕРЕХОДЕ В ПОРИСТОЙ ПЛАСТИНЕ

Аннотация—Выполнено аналитическое исследование взаимосвязанного тепло-и массопереноса при фазовом превращении в пористой пластине. Обнаружено два пространственно устойчивых режима, которые соответствуют неподвижному и подвижному состояниям конденсата. Получены аналитические выражения в замкнутом виде для определения полей температуры, концентрации пара, скорости конденсации и влагосодержания, а также местоположения области конденсации для каждого из режимов.